Thermochimica Acta, 63 (1983) 307–316
Elsevier Science Publishers B.V., Amsterdam – Printed in The Netherlands

THE KINETICS AND THERMODYNAMICS OF THE THERMAL PYRIDINE DISSOCIATION OF BIS(PYRIDINE)BIS(*N*-ALKYL-SUBSTITUTED-SALICYLIDENEAMINATO)NICKEL(II) IN THE SOLID STATE. KINETIC AND THERMODYNAMIC BOND STABILITIES

H. MASUDA, T. KAWARADA, K. MIYOKAWA and I. MASUDA

Department of Chemistry, Faculty of Science, Fukuoka University, Nanakuma, Jonan-ku, Fukuoka 814-01 (Japan)

(Received 6 October 1982)

ABSTRACT

Thermal pyridine dissociation reactions of the bis-pyridine adducts of bis(*N*-alkyl-substituted-salicylideneaminato)nickel(II), abbreviated as Ni(*N*-R-X-salam)$_2$py$_2$ (R = Me; X = 5-MeO, 5-Me, H, 5-F, 5-Cl, 5-Br, 5-NO_2: X = H; R = Et, *n*-Pr, i-Pr, *n*-Bu, i-Bu, *n*-pentyl, *n*-hexyl, *n*-heptyl, cyclohexyl), were characterized by means of TG, DSC, and isothermal weight-loss measurements. These adducts dissociated 2 moles of pyridine per mole of the adduct at one stage in the temperature range 350–470 K; the depyridination reactions for the adducts including R = i-Pr or i-Bu gave rise to pseudo-tetrahedral parent complexes and those for the remaining adducts gave square-planar parent complexes. The ΔH values, heat of depyridination, varied in the range 98–165 kJ mole^{-1}, depending on the nature of R and X. Kinetic analyses revealed that for all the adducts the reactions followed the contracting-disc equation. The logarithmic values of the rate constants at 350 K linearly decreased with an increase in ΔH values, indicating that kinetic bond stability could be correlated with thermodynamic bond stability with respect to the Ni(II)–pyridine linkage. It was also shown that on substituting X on the aryl rings the Ni(II)–pyridine bond strength was influenced predominantly by the electronic effect of X, and on substituting R on the imine nitrogen atoms the bond strength was influenced predominantly by the steric effect of R.

INTRODUCTION

The bond stability of metal–ligand linkage in the coordination compounds has often been discussed in terms of the initial temperature of the thermal ligand dissociation reaction observed in thermoanalytical curves such as TG or DTA/DSC [1]. Although the bond stability expressed with such an initial temperature reflects the kinetic features of the reaction, it does not necessarily reflect the thermodynamic feature of the bond stability. In fact, several works dealing with both kinetic and thermodynamic bond stabilities have suggested that the initial temperature does not always corre-

0040-6031/83/$03.00

spond to the thermodynamic bond stability [2–4]. Since the observed initial temperature on the thermoanalytical curve is to be affected by the experimental conditions and the reaction mechanism, the kinetic bond stability

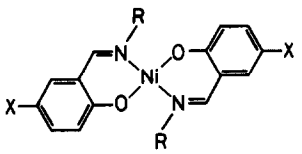

Fig. 1. Ni(*N*-R-X-salam)$_2$.

should be described more strictly by using a rate constant at a normalized, definite temperature. Then, it is thought to be significant to examine the relation between the kinetic bond stability denoted in this manner and the thermodynamic bond stability.

In the present work, thermal analysis has been carried out on the thermal pyridine dissociation reactions in the solid phase of a series of adduct complexes, bis(pyridine)bis(*N*-alkyl-substituted-salicylideneaminato)nickel(II) shown in Fig. 1, abbreviated hereafter as Ni(*N*-R-X-salam)$_2$py$_2$. The reaction rates and the heats of reaction are discussed in connection with both the kinetic and thermodynamic bond stabilities for the linkage between the central Ni(II) ion and pyridine.

EXPERIMENTAL

The pyridine adducts, Ni(*N*-R-X-salam)$_2$py$_2$, were prepared as described elsewhere [5] and were identified by means of nickel and pyridine analyses.

The TG and DSC curves were recorded on a Rigaku Denki 8002 thermal analyzer at a heating rate of 10 K min^{-1} in a flowing nitrogen atmosphere. α-Al_2O_3 was used as reference material. The ΔH value, the heat of dissociation of pyridine from the adduct, was determined by measuring the DSC peak area following the method of Beech et al. [2]. The instrument was calibrated against the heat of transition of potassium nitrate [6]. The data listed in Table 1 are given as mean values of more than three measurements, and the associated uncertainties are the standard deviations from the mean values. The kinetic analyses of the depyridination reactions were carried out on the basis of the weight-loss curves; these were recorded under isothermal and dynamic (heating rate 1 K min^{-1}) conditions on a Sinku Riko TGD-3000-RH thermal analyzer in a flowing nitrogen atmosphere. Coats and Redfern's method [7] was employed for the dynamic weight-loss curve analyses. A 15–20 mg aliquot of the sample (particle size 200–250 mesh) was provided in each run.

TABLE 1

Thermal and kinetic remarks for the depyridination reaction of Ni(*N*-R-X-salam)$_2$py$_2$

Adduct			Thermal analysis					Kinetic analysis				
No.	X	R	TG Weight loss [a]	DSC				Isothermal		Dynamic		
				T_i [b]	T_m [b]	T_f [b]	ΔH [c]	E_a [d]	log A [e]	E_a [d]	log A [e]	$-\log k_{350}$ [f]
1	5-MeO	Me	28.96(29.01)	337	371	385	115 ± 1	72.6 ± 4.9	9.1 ± 0.7	73.3 ± 0.2	9.4 ± 0.1	1.54
2	5-Me	Me	29.98(30.82)	340	371	384	121 ± 1	89.0 ± 10.9	11.4 ± 1.6	79.7 ± 0.5	10.2 ± 0.1	1.69
3	H	Me	33.64(32.61)	348	406	423	131 ± 2	85.8 ± 2.8	10.5 ± 0.4	82.4 ± 0.4	10.1	2.20
4	5-F	Me	29.95(30.35)	350	400	421	127 ± 3	66.5 ± 9.6	7.9 ± 1.3	69.0 ± 0.3	8.1 ± 0.1	2.20
5	5-Cl	Me	29.02(28.55)	360	432	454	147 ± 3	81.0 ± 3.9	9.2 ± 0.5	82.8 ± 0.3	9.4 ± 0.1	2.96
6	5-Br	Me	24.17(24.61)	370	427	449	140 ± 7	83.8 ± 10.3	9.6 ± 1.4	81.3 ± 0.5	9.6 ± 0.1	2.53
7	5-NO_2	Me	27.02(27.50)	400	458	477	165 ± 2	93.9 ± 3.6	10.3 ± 0.5	96.1 ± 1.0	10.5 ± 0.1	3.84
8	H	Et	30.29(30.82)	344	392	410	125 ± 6			82.8 ± 0.7	10.4 ± 0.1	1.96
9	H	*n*-Pr	28.27(29.23)	346	398	419	116 ± 3			71.0 ± 0.6	8.7 ± 0.1	1.90
10	H	*i*-Pr	28.40(29.23)	350	402	417	110 ± 2			80.4 ± 1.4	9.9 ± 0.1	2.10
11	H	*n*-Bu	27.52(27.79)	345	380	(395)				76.7 ± 0.4	9.5 ± 0.1	1.95
12	H	*i*-Bu	26.92(27.79)	349	397	414	112 ± 3			76.3 ± 1.1	9.3 ± 0.2	2.09
13	H	*n*-Pentyl	25.66(26.48)	327	365	(385)				86.6 ± 2.7	11.5 ± 0.4	1.42
14	H	*n*-Hexyl	24.24(25.29)	323	351	(373)				91.6 ± 2.5	12.4 ± 0.4	1.27
15	H	*n*-Heptyl	24.01(24.21)	330	354	(369)				78.5 ± 3.1	10.3 ± 0.6	1.42
16	H	Cyclohexyl	25.31(25.46)	336	383	403	98 ± 2			99.3 ± 1.8	13.2 ± 0.3	1.62

[a] Calculated values (%) are given in parentheses.

[b] T_i, T_m, and T_f denote, respectively, the initial, maximum and final temperatures (K) of the DSC peak due to depyridination.

[c] Heat of depyridination (kJ mole^{-1}).

[d] Activation energy (kJ mole^{-1}).

[e] A Pre-exponential factor (s^{-1})

[f] k_{350} = Rate constant at 350 K (s^{-1}).

RESULTS

The bis-pyridine adducts subjected to the present investigation are listed in Table 1. These showed the magnetic moments, $\mu_{eff} = 3.09–3.31$ μ_B at 298 K, as expected for Ni(II) complexes with octahedral coordination [8]. Their electronic spectra were composed of two peaks with the maxima at ca. 10.0 and 17.0×10^3 cm^{-1}; these could be ascribed, respectively, to the $^3A_{2g} \rightarrow {}^3T_{2g}$ and $^3A_{2g} \rightarrow {}^3T_{1g}(F)$ transitions of the Ni(II) ion in the octahedral crystal field [9]. It was noted that these positions scarcely varied when the substituents R and X were different within the series of the present adducts.

The TG and DSC curves indicated that 1 mole of the respective adducts liberated endothermally 2 moles of pyridine at one stage in the temperature range 350–470 K and no intermediary formation of a mono-pyridine adduct occurred. These findings agree with the thermoanalytical results for Ni(*N*-Bu-X-salam)$_2$py$_2$ (X = H and Cl) complexes [10] and for the Ni(*N*-[R-C_6H_4]salam)$_2$py$_2$ (R = 4-MeO, 4-Me, H, 4-F, 4-Cl, and 4-Br) complexes [5]. The depyridination of these adducts other than **10** and **12** produced the diamagnetic parent complexes Ni(*N*-R-X-salam)$_2$ with square-planar coordination, while that of adducts **10** and **12** gave the paramagnetic parent complexes with pseudo-tetrahedral coordination. As for the latter two cases, their authentic parent complexes isolated from the solution are also paramagnetic with pseudo-tetrahedral coordination [11]. Thus, the depyridination reactions are accompanied by a change in the coordination structure around the Ni(II) ion, i.e. from octahedral to square-planar for the former and from octahedral to pseudo-tetrahedral for the latter adducts.

The ΔH values for the depyridination reactions are listed in Table 1; for adducts **11** and **13–15**, their ΔH values could not be determined as the DSC peak was overlapped by that due to the melting of the resultant parent complex.

The kinetic analyses for the depyridination reactions carried out on the isothermal weight-loss curves for adducts **1–7** indicated that the reactions fit fairly well the contracting-disc equation

$$1 - (1 - \alpha)^{1/2} = kt$$

where α, k, and t denote the molar fraction of the adduct which liberated pyridine, the rate constant, and the time, respectively. This is exemplified with the results obtained for adduct **3** in Fig. 2. Figure 3 shows the Arrhenius plots. The activation energy, E_a, and pre-exponential factor, A, given in Table 1 are those calculated from the slope and the vertical intercept of a straight line in Fig. 3 by means of the least-squares method. The dynamic weight-loss curve analyses carried out using the method of Coats and Redfern also indicated that the reactions follow the contracting-disc equation, as shown in Figs. 4 and 5. Then the E_a and A values given in

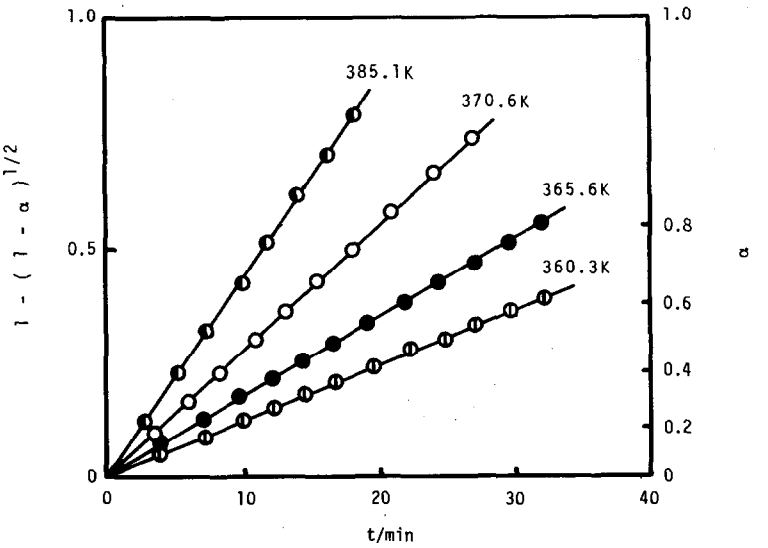

Fig. 2. Contracting-disc rate plots for the depyridination reaction of adduct **3** under isother mal conditions.

Table 1 are calculated by using the relationship [7]

$$\ln\left[2\left(1-(1-\alpha)^{1/2}\right)/T^2\right] = \ln\left[AR/\beta E_a(1-2RT/E_a)\right] - E_a/RT$$

where β is the heating rate, and R is the gas constant. Good agreement i seen in both E_a and A values which were determined by the above tw methods.

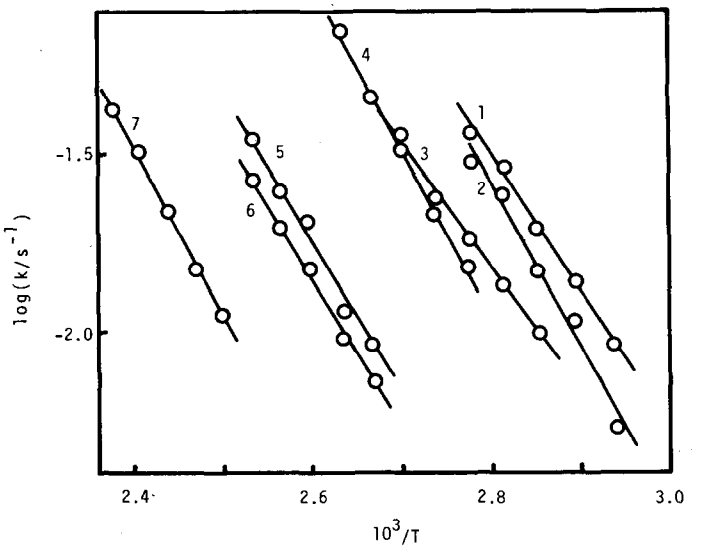

Fig. 3. Arrhenius plots for the depyridination reactions of adducts **1–7**.

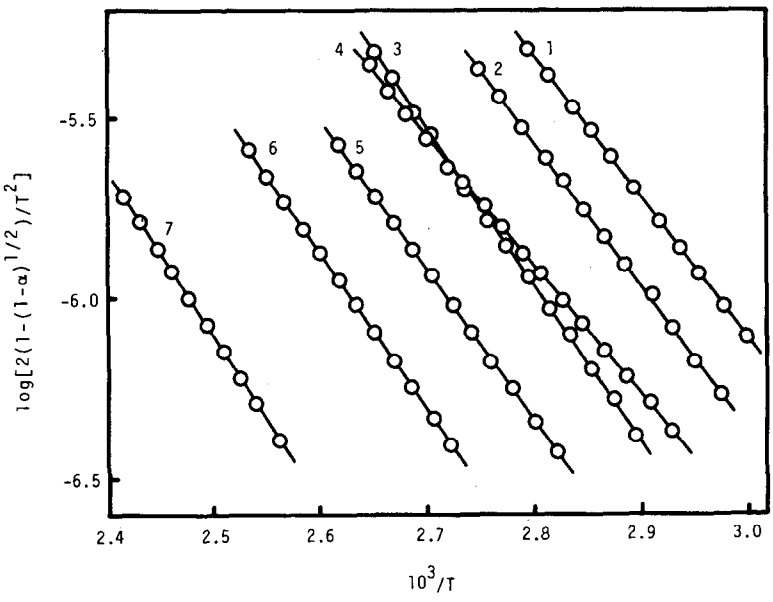

Fig. 4. Rate plots for the depyridination reactions of adducts **1–7** under dynamic conditions.

For adducts **8–16**, their kinetic parameters are those determined from the dynamic data.

In order to compare the rate constants they should be normalized. The values at 350 K are taken here; at this temperature all adducts undergo the

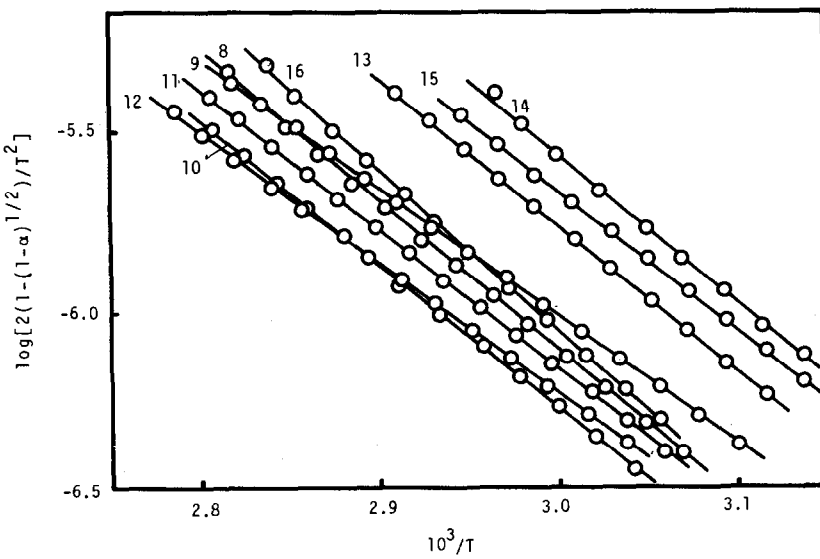

Fig. 5. Rate plots for the depyridination reactions of adducts **8–16** under dynamic conditions.

depyridination reaction. The logarithmic values of k_{350} given in Table 1 are calculated from the E_a and A values determined under dynamic conditions. It is seen from Table 1 that not only the initial temperature but also the maximum temperature in the DSC curves can be related to the log k_{350} values.

DISCUSSION

Thermodynamic and kinetic bond stabilities

Although a large number of transition-metal compounds have been coordinated with the volatile, neutral molecular ligand, only a few kinetic and/or thermodynamic data on the thermal dissociation of the volatile ligand have so far been reported. Beech et al. [2] have shown that in the reaction

$$NiX_2py_4(\text{solid}) \rightarrow NiX_2py_2(\text{solid}) + 2\ py(\text{gas})\ (X = Cl, Br, \text{and } I)$$

the ΔH values fall in the range 100–143 kJ mole^{-1}, the ΔH values, 98–165 kJ mole^{-1}, found for the present adducts are in a similar range.

It may be considered that in practice the ΔH values determined in the present investigation are the mean values of the enthalpy change over the temperature range of the DSC peak for the depyridination reaction

$$Ni(N\text{–R–X–salam})_2py_2(\text{solid}) \rightarrow Ni(N\text{–R–X–salam})_2(\text{solid}) + 2\ py(\text{gas})$$

In order to describe precisely the thermodynamic Ni(II)–pyridine bond stability, the ΔH_f value, enthalpy change in the following gas phase reaction, should be adopted

$$Ni(N\text{–R–X–salam})_2(\text{gas}) + 2\ py(\text{gas}) \rightarrow Ni(N\text{–R–X–salam})_2py_2(\text{gas})$$

The ΔH_f value is related to the ΔH value as

$$\Delta H_f = -\Delta H + [\Delta H_{sub}(Ni(N\text{–R–X–salam})_2py_2) - \Delta H_{sub}(Ni(N\text{–R–X–salam})_2)]$$

where ΔH_{sub} represents the enthalpy of sublimation for the respective compounds. Actually the ΔH_{sub} values could not be easily determined. However, it is probable that in a series of complexes with analogous ligands the differences in the ΔH_{sub} values do not vary much with different ligands [2]. If this assumption is accepted, the ΔH values may be taken as a measure of the thermodynamic bond stability of the Ni(II)–pyridine bonding.

As shown in Fig. 6, the plots of ΔH vs. $-\log k_{350}$ indicate that ΔH increases linearly as $-\log k_{350}$ increases, i.e., the thermodynamic characteristic is closely related to the reaction rate. The relation obtained here is thought to be further supported by the fact that the same reaction scheme, i.e. contracting-disc equation, is adopted for the reactions of all the com-

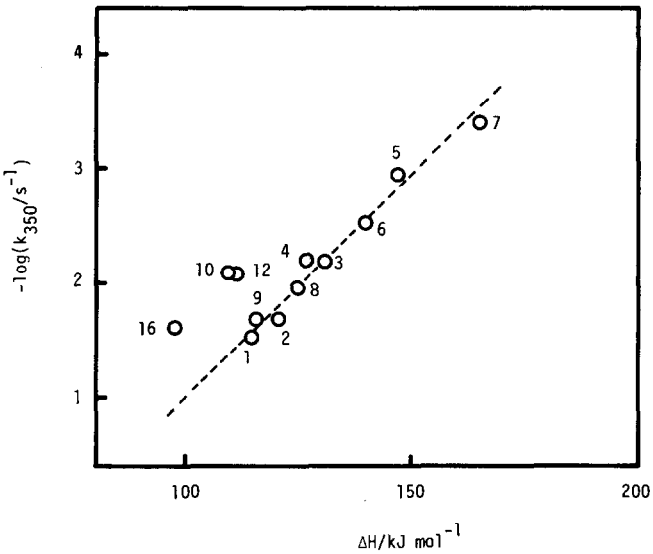

Fig. 6. The relationship between ΔH and $-\log k_{350}$ values.

plexes investigated here. The reaction rates of the thermal ligand dissociation of the coordination compounds are not always determined only by the process of their metal–ligand bond cleavage, but are often determined by the diffusion process of the liberated gaseous ligands. Therefore, without taking into account kinetic analyses data, the initial temperatures of the reactions observed in TG or DTA/DSC curves should not be related to the metal–ligand bond stabilities.

Effect of the nature of substituents X and R on the Ni(II)–pyridine bonding

Previously, we have reported that in the Ni(*N*-(Y_6-C_6H_4)salam)$_2$py$_2$ complexes electron-withdrawing Y increases the Lewis acidity of the Ni(II) and hence increases the activation energies for the thermal depyridination reactions [5]. As Table 1 shows, this tendency is also observed in the present adduct complexes on substituting X on the aryl rings. For adducts 1–7 the ΔH values correlate linearly with Hammett's *para*-substitution constant σ_p of X [12], as shown in Fig. 7. The electron-releasing methyl group decreases the ΔH value, while the electron-withdrawing nitro group increases it. Similar plots against σ_m values gave a rather scattered relation. These facts indicate that the substituents transmit their electronic effects predominantly via the phenolato oxygen atoms to Ni(II). Unfortunately, there is no thermodynamic data in solution with which the present data for the solid state could be compared. The $-\log k_{350}$ values also increase linearly with an increase in the σ_p values, as seen in Fig. 6. The Ni(II)–pyridine bonding in the present adducts is generally considered to occur through the σ-donation of pyridine to the Ni(II) and the π-electron back-donation from the Ni(II) to pyridine. A

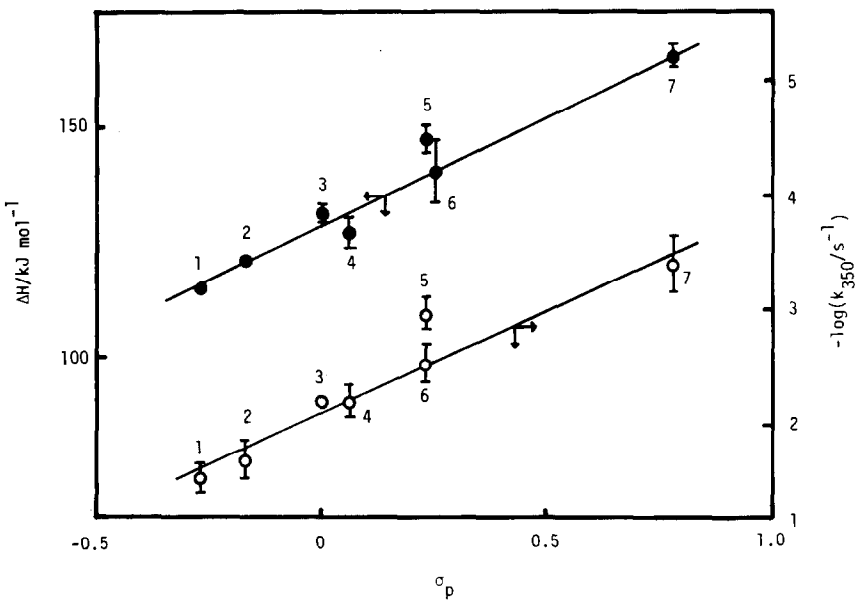

Fig. 7. Plots of ΔH and $-\log k_{350}$ against Hammett's σ_p values for adducts **1**–**7**.

positive slope in the ΔH vs. σ_p plots suggests that the Ni(II)–pyridine bond stability is dominated by the σ-donation, i.e. the electron-withdrawing substituent X reduces the electron density on the Ni(II) and facilitates the σ-electron donation of pyridine.

It is seen from Table 1 that the changes in the $-\log k_{350}$ values for adducts **3** and **8**–**16**, including a series of *N*-alkyl substituents R, are so large that these changes cannot be ascribed only to the electronic effects of R. Moreover, a noticeable relation was not seen between the $-\log k_{350}$ values and the inductive substitution constants of R [13]. It is observed that a decrease in the electron-donating property of R rather causes an increase in the $-\log k_{350}$ values. Therefore, alkyl groups in the adducts seem to exert their steric effects toward pyridine coordination. Adducts **10** and **12** having α-branched R are different from the remaining adducts; upon pyrolyses they gave rise to the tetrahedral parent complexes. In the ΔH vs. $-\log k_{350}$ plots in Fig. 5, their plots deviate from a straight line. The $-\log k_{350}$ values for **10** and **12** are larger than those for **9** and **11** with the normal alkyl chain groups. It is of interest to refer to the solution equilibrium data by Schumann et al [14]: in toluene solution the adduct formation constants for **10** and **12** are larger than those for **8**, **9** and **11**.

REFERENCES

1 A.E. Newkirk, Anal. Chem., 32 (1960) 1558.
C.J. Keattch and D. Dollimore, An Introduction to Thermogravimetry, Heyden, London, 1975, pp. 25–51.
2 G. Beech, C.T. Mortimer and E.G. Tyler, J. Chem. Soc. A, (1967) 925.
G. Beech, S.J. Ashcroft and C.T. Mortimer, J. Chem. Soc. A, (1967) 929.
G. Beech, C.T. Mortimer and E.G. Tyler, J. Chem. Soc. A, (1967) 1111.
G. Beech and C.T. Mortimer, J. Chem. Soc. A, (1967) 1115.
3 K. Nagase, K. Muraishi, K. Sone and N. Tanaka, Bull. Chem. Soc. Jpn., 48 (1975) 3184.
4 G. Hakvoort, J.C. van Dam and J. Reedijk, Proc. 5th Int. Conf. Therm. Anal., 1977, p. 186.
5 K. Miyokawa, H. Hirashima and I. Masuda, Bull. Chem. Soc. Jpn., 55 (1982) 104.
6 W.W. Wendlandt, Thermal Methods of Analysis, Wiley, New York, 2nd edn., 1974, p. 184.
7 A.W. Coats and J.P. Redfern, Nature (London), 201 (1964) 68.
8 B.N. Figgis and J. Lewis, Prog. Inorg. Chem., 6 (1964) 37.
9 A.B.P. Lever, Inorganic Electronic Spectroscopy, Elsevier, Amsterdam, 1968, p. 333.
10 D.R. Dakternieks, D.P. Gordon, L.F. Lindoy and G.M. Mockler, Inorg. Chim. Acta, 7 (1973) 467.
11 R.H. Holm, G.W. Everett, Jr. and A. Chakravatry, Prog. Inorg. Chem., 7 (1966) 83.
12 H.H. Jaffe, Chem. Rev., 53 (1953) 191.
13 R.W. Taft, Jr., Steric Effects in Organic Chemistry, John Wiley, New York, 1956, p. 556.
14 M. Schumann, A. von Holtum, K.J. Wannowius and H. Elias, Inorg. Chem., 21 (1982) 606.